Optimization of Advanced Sliding Mode Controllers Using Genetic Algorithms for Enhanced Magnetic Levitation System Performance

BELGACEM BEKKAR, KHALED FERKOUS
Materials, Energy Systems Technology and Environment Laboratory,
University of Ghardaia,
ALGERIA

Abstract: - Magnetic levitation systems are nonlinear and open-loop unstable, which makes accurate and robust control difficult. This paper investigates two sliding-mode-based controllers for a nonlinear MagLev system: the Super-Twisting Sliding Mode Controller (STSMC) and a Conditioned Barrier Adaptive Function Double-Integral Terminal Super-Twisting Sliding Mode Controller (CB-STSMC). Both controllers are designed to regulate the levitation gap while ensuring proper tracking of magnetic flux and momentum states. Their gains are optimized using a Genetic Algorithm with the Integral of Time-weighted Absolute Error as the fitness criterion. Closed-loop stability is established through Lyapunov analysis. MATLAB/Simulink results show that both controllers achieve stable levitation, while the proposed CB-STSMC provides faster convergence, smaller overshoot, and improved disturbance rejection compared with the conventional STSMC. These results confirm the effectiveness of the proposed strategy for robust and precise nonlinear MagLev control.

Key-Words: - Magnetic levitation, Super-Twisting Sliding Mode Control, Conditioned Barrier Adaptive Function, Terminal Sliding Mode Control, Genetic algorithm optimization, advanced sliding Mode controllers.

Received: May 26, 2025. Revised: July 19, 2025. Accepted: September 25, 2025. Published: June 1, 2026.

1 Introduction

Magnetic Levitation (MagLev) technology is revolutionizing transportation by enabling high-speed, efficient, and sustainable mobility solutions, [1], [2]. MagLev systems use electromagnetic forces to lift and propel vehicles without direct mechanical contact with tracks or guideways, thereby significantly reducing friction and mechanical wear. This technology has been widely investigated in advanced transit systems and experimental transportation platforms, where the absence of mechanical contact allows higher operational speeds and smoother motion.

The fundamental operating principle of MagLev systems relies on applying an electric voltage to an electromagnet to generate a magnetic force capable of counteracting gravitational forces, [3]. This electromagnetic force enables the suspension of ferromagnetic objects in mid-air without physical contact, eliminating friction-induced energy losses. The contactless nature of MagLev technology also reduces maintenance requirements and increases system lifespan, contributing to improved reliability and durability.

Despite these advantages, the intrinsic nonlinear dynamics of MagLev systems introduce significant challenges in controller design, [4]. Conventional linear controllers typically operate effectively only around limited linearized operating points and therefore struggle to maintain performance across the full nonlinear operating range. Consequently, the development of robust nonlinear control strategies is required to ensure fast dynamic response, limited overshoot, and effective disturbance rejection.

Recent research has explored several nonlinear control approaches, including Fuzzy Logic Controllers (FLC) and Artificial Neural Networks (ANN), [5], [6]. While these methods have shown promising results, they may suffer from slow convergence and sensitivity to external disturbances. To address these limitations, this work investigates a CB-STSMC, [7], [8]. This control strategy is designed to reduce chattering while improving transient performance and tracking accuracy. In addition, recent implementations of backstepping control for MagLev systems, [9], have demonstrated systematic stability properties; however, they often exhibit relatively large steady-state errors, which are only partially mitigated by integral backstepping schemes.

Motivated by these limitations, the present study proposes the use of the CB-STSMC algorithm to enhance the dynamic performance of the MagLev system. The controller is designed to improve the tracking of desired state variables while minimizing the ITAE. To further enhance control performance, the parameters of the CB-STSMC controller are optimized using a GA. This optimization approach provides an effective mechanism for tuning controller gains, enabling improved performance across varying operating conditions.

The remainder of this paper is organized as follows. Section 2 presents the mathematical model of the MagLev system. Section 3 describes the controller design, including the STSMC and the proposed CB-STSMC. Section 4 reports the simulation setup and results, including the GA-based optimization of controller gains and a comparative performance analysis. Finally, Section 5 concludes the paper and outlines potential directions for future research.

2 Mathematical Modeling of the MagLev System

The mathematical modeling of a MagLev system requires describing the dynamics of a ferromagnetic ball suspended in a vertical magnetic field generated by an electromagnet. The behavior of this electromechanical system is governed by the interaction between electromagnetic and mechanical dynamics. The model is therefore derived using principles from electromagnetism and classical mechanics, emphasizing the relationships between magnetic flux, coil current, and the resulting mechanical forces acting on the levitated object, [9], [10].

2.1 System Description

Consider a MagLev system in which an iron ball is suspended in a vertical magnetic field produced by an electromagnet, as illustrated in Figure 1, [11]. The magnetic circuit is assumed to operate in the unsaturated region, which implies that the magnetic flux λ varies linearly with the coil current i and the ball position θ.

The variable θ denotes the vertical displacement of the ball from its nominal equilibrium position, measured along the vertical axis and oriented downward.

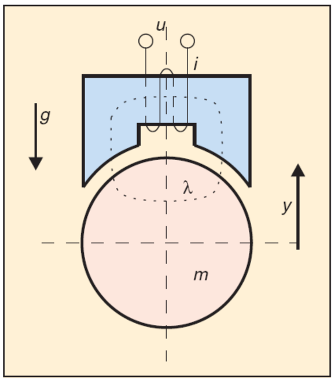

Fig. 1: Schematic representation of the magnetic levitation system ($y = \theta$),
Source: [11]

2.2 Governing Equations

The dynamics of the MagLev system are described using Kirchhoff's voltage law for the electrical circuit and Newton's second law for the mechanical motion of the levitated ball.

Applying Kirchhoff's voltage law to the electromagnet coil yields:

$$u = \frac{d\lambda}{dt} + Ri \tag{1}$$

where u denotes the applied voltage, R is the coil resistance. The vertical motion of the levitated ball is governed by Newton's second law:

$$m\frac{d^2\theta}{dt^2} = F - mg \tag{2}$$

where m is the mass of the ball, g is the gravitational acceleration, and F denotes the electromagnetic force generated by the coil.

The electromagnetic force is obtained from the magnetic energy stored in the inductive field and can be expressed as:

$$F = \frac{1}{2}\frac{dL(\theta)}{d\theta}i^2 \tag{3}$$

where $L(\theta)$ is the position-dependent inductance of the electromagnet.

The inductance is commonly approximated by $L(\theta) = \frac{k}{1-\theta}$ where k is a constant related to the magnetic circuit parameters.

Since the magnetic flux is defined as:

$$\lambda = L(\theta)i \tag{4}$$

the coil current can be written as:

$$i = \frac{\lambda}{L(\theta)} = \frac{(1-\theta)}{k}\lambda$$

Substituting this expression into Eq. (1) yields:

$$u = \frac{d\lambda}{dt} + \frac{(1-\theta)R}{k}\lambda \tag{5}$$

Substituting the electromagnetic force expression from Eq. (3) into Eq. (2) gives:

$$m\frac{d^2\theta}{dt^2} = \frac{1}{2}\frac{dL(\theta)}{d\theta}i^2 - mg \qquad (6)$$

The momentum of the levitated ball is defined as:

$$\rho = m\frac{d\theta}{dt} \qquad (7)$$

which leads to

$$\frac{d\rho}{dt} = \frac{1}{2}\frac{dL(\theta)}{d\theta}i^2 - mg \qquad (8)$$

The derivative of the inductance with respect to the position is:

$$\frac{dL(\theta)}{d\theta} = \frac{k}{(1-\theta)^2} \qquad (9)$$

Substituting Eq. (9) into Eq. (8) results in:

$$\frac{d\rho}{dt} = \frac{1}{2}\frac{k}{(1-\theta)^2}i^2 - mg \qquad (10)$$

Using the flux relation in Eq. (4), the previous equation can be rewritten as:

$$\frac{d\rho}{dt} = \frac{\lambda^2}{2k} - mg \qquad (11)$$

The complete nonlinear model of the MagLev system can therefore be obtained from Eqs. (5), (7), and (11). Defining the state vector:

$$x = [x_1\ x_2\ x_3]^T = [\theta\ \rho\ \lambda]^T$$

the system can be expressed in the following state-space form

$$\dot{x}_1 = \frac{x_2}{m} \qquad (12)$$

$$\dot{x}_2 = \frac{x_3^2}{2k} - mg \qquad (13)$$

$$\dot{x}_3 = -\frac{(1-x_1)R}{k}x_3 + u \qquad (14)$$

This nonlinear state-space representation is suitable for the design of advanced nonlinear controllers.

3 Controller Design

The MagLev system described by Eqs. (12)–(14) exhibits strong nonlinear behavior due to the presence of the quadratic term x_3^2 in the mechanical dynamics and the product term $(1-x_1)x_3$in the electrical subsystem. These nonlinearities make the stabilization of the levitated ball particularly challenging when using conventional linear control strategies. Therefore, the design of a robust nonlinear controller is required to ensure accurate regulation of the levitation gap and stable system operation.

The feedback control structure used in this study is illustrated in Figure 2. The controller operates by regulating the error between the desired and measured position of the levitated ball. Based on this feedback, the control input voltage applied to the electromagnet is adjusted to maintain stable levitation and desired system dynamics.

The proposed controllers are designed to satisfy the following control objectives:

1) Maintain the desired levitation gap between the electromagnet and the ball.
2) Ensure accurate tracking of the reference magnetic flux required to sustain the levitation force.
3) Drive the ball momentum to zero to eliminate residual oscillations.
4) Guarantee asymptotic stability of the closed-loop system.

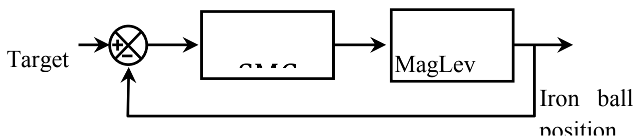

Fig. 2: Control flow diagram for MagLev System
Source: created by the authors

3.1 Super-Twisting Sliding Mode Control (STSMC)

In the design of a STSMC algorithm, the selection of an appropriate sliding surface represents a fundamental step. Several approaches have been proposed for constructing sliding surfaces in nonlinear control systems, [12]. Among these methods, error-based sliding surfaces are widely adopted due to their simplicity and ease of implementation. Therefore, this approach is employed in the present study to improve the tracking of the desired state variables of the MagLev system.

The tracking errors between the actual and reference states are defined as:

$$e_i = x_i - x_{i\,ref} \qquad (15)$$

where $x_{i\,ref}(i = 1{,}2{,}3)$ denote the reference values corresponding to the desired air gap, momentum, and magnetic flux, respectively.

Taking the time derivative of Eq. (15) yields:

$$\dot{e}_i = \dot{x}_i - \dot{x}_{iref} \qquad (16)$$

The sliding surface is then defined as a linear combination of the tracking errors:

$$s = c_1e_1 + c_2e_2 + c_3e_3 \qquad (17)$$

where c_1, c_2, and c_3 are positive design constants.

Differentiating Eq. (17) with respect to time gives:

$$\dot{s} = c_1\dot{e}_1 + c_2\dot{e}_2 + c_3\dot{e}_3 \tag{18}$$

Substituting the state-space dynamics given in Eqs. (12)–(14) and the error derivatives from Eq. (16) into Eq. (18) result in:

$$\begin{aligned}\dot{s} &= c_1\left(\frac{x_2}{m} - \dot{x}_{1ref}\right) + c_2\left(\frac{x_3^2}{2k} - mg - \dot{x}_{2ref}\right) \\ &+ c_3\left(-\frac{R(1-x_1)x_3}{k} + u - \dot{x}_{3ref}\right)\end{aligned} \tag{19}$$

Setting $\dot{s} = 0$ in Eq. (19) yields the equivalent control input:

$$\begin{aligned}u_{eq} = -\frac{1}{c_3}\bigg[&c_1\left(\frac{x_2}{m} - \dot{x}_{1ref}\right) + c_2\left(\frac{x_3^2}{2k} - mg - \dot{x}_{2\text{ref}}\right) \\ &+ c_3\left(-\frac{R(1-x_1)x_3}{k} - \dot{x}_{3ref}\right)\bigg]\end{aligned} \tag{20}$$

The discontinuous component of the STSMC control law is defined as:

$$u_{sw} = -k_1 \mid s \mid \, sgn(s) - k_2 \int sgn(s)\, dt \tag{21}$$

where the sign function is defined as:

$$sgn(s) = \begin{cases} -1 & s < 0 \\ 0 & s = 0 \\ 1 & s > 0 \end{cases} \tag{22}$$

The control gains $k_1$and $k_2$are key parameters of the STSMC algorithm. The gain k_1 determines the magnitude of the discontinuous control action, while k_2 regulates the integral component of the super-twisting algorithm. Proper tuning of these parameters is necessary to ensure stability and improve tracking performance, [13], [14]. In this work, the parameters are optimized using a GA to enhance robustness and tracking accuracy.

The complete STSMC control law is therefore expressed as:

$$u = u_{eq} + u_{sw} \tag{23}$$

Substituting Eqs. (20) and (21) into Eq. (23) gives:

$$\begin{aligned}u = -\frac{1}{c_3}\bigg[&c_1\left(\frac{x_2}{m} - \dot{x}_{1ref}\right) + c_2\left(\frac{x_3^2}{2k} - mg - \dot{x}_{2ref}\right) \\ &+ c_3\left(-\frac{R(1-x_1)x_3}{k} - \dot{x}_{3ref}\right)\bigg] \\ &- k_1|s|sgn(s) - k_2\int sgn(s)\, dt\end{aligned} \tag{24}$$

To analyze the stability of the closed-loop system, the following Lyapunov candidate function is considered, [15]:

$$V = \frac{1}{2}s^2 \tag{25}$$

Taking the time derivative of Eq. (25) yields:

$$\dot{V} = s\dot{s} \tag{26}$$

Substituting the expression of $\dot{s}$ and applying the control law in Eq. (24) leads to:

$$\dot{V} = -k_1 \mid s \mid^2 - k_2 \mid s \mid \leq 0 \tag{27}$$

Since $\dot{V}$ is negative semi-definite, the sliding variable s converges to zero, and the asymptotic stability of the closed-loop system is ensured under the proposed STSMC control law.

3.2 Conditioned Barrier Adaptive Function Double Integral Terminal Super-Twisting Sliding Mode Control (CB-STSMC)

The CB-STSMC is an advanced control strategy developed to enhance the performance and robustness of MagLev systems in the presence of nonlinear dynamics, steady-state errors, and external disturbances, [8]. This control framework combines several mechanisms within a unified structure.

The conditioned barrier mechanism introduces operational constraints that prevent the system states from entering unstable regions. The adaptive component continuously adjusts the controller parameters in response to variations in system dynamics and environmental conditions, thereby maintaining consistent control performance. In addition, the double-integral terminal structure improves tracking accuracy and accelerates convergence toward the desired equilibrium point while reducing steady-state errors. The integration of super-twisting sliding mode principles further enhances robustness against disturbances and model uncertainties, enabling stable and precise control of the levitated ball.

The error variables and their derivatives are defined in Eqs. (15) and (16). To improve error compensation and enhance convergence behavior, the integral of the error signals is introduced as:

$$\begin{aligned} e_4 &= \int e_1\, dt \\ e_5 &= \int e_2\, dt \\ e_6 &= \int e_3\, dt \end{aligned} \tag{28}$$

To further reduce steady-state error and suppress oscillatory behavior, double-integral terms of the tracking errors are also incorporated:

$$\begin{aligned} e_7 &= \int \left(\int e_1\, dt \right) dt \\ e_8 &= \int \left(\int e_2\, dt \right) dt \\ e_9 &= \int \left(\int e_3\, dt \right) dt \end{aligned} \tag{29}$$

The sliding surface incorporating proportional, integral, and double-integral error components is defined as:

$$\begin{gathered} s = c_1 e_1 + c_2 e_2 + c_3 e_3 \\ +c_4 (e_4)^{q_1} + c_5 (e_5)^{q_2} + c_6 (e_6)^{q_3} \\ +c_7 e_7 + c_8 e_8 + c_9 e_9 \end{gathered} \tag{30}$$

where $c_i (i = 1, \ldots, 9)$ are positive design parameters and q_1, q_2, q_3 are fractional powers used to improve convergence properties.

Taking the time derivative of Eq. (30) yields:

$$\begin{gathered} \dot{s} = c_1 \dot{e}_1 + c_2 \dot{e}_2 + c_3 \dot{e}_3 + \\ c_4 q_1 e_4^{q_1 - 1} e_1 + c_5 q_2 e_5^{q_2 - 1} e_2 + c_6 q_3 e_6^{q_3 - 1} e_3 \\ +c_7 e_4 + c_8 e_5 + c_9 e_6 \end{gathered} \tag{31}$$

Setting $\dot{s} = 0$ and substituting the system dynamics from Eqs. (12)–(14) results in the equivalent control input:

$$\begin{gathered} u_{eq} = -\frac{1}{c_3}\Big[c_1 \left(\frac{x_2}{m} - \dot{x}_{1ref} \right) + c_2 \left(\frac{x_3^2}{2k} - mg - \dot{x}_{2ref} \right) \\ c_3 \left(-\frac{R(1 - x_1) x_3}{k} - \dot{x}_{3ref} \right) + c_4 q_1 e_4^{q_1 - 1} e_1 + c_5 q_2 e_5^{q_2 - 1} e_2 \\ +c_6 q_3 e_6^{q_3 - 1} e_3 + c_7 e_4 + c_8 e_5 + c_9 e_6 \Big] \end{gathered} \tag{32}$$

To ensure that the system trajectories reach and remain on the sliding surface, a reaching law is introduced, [12]. The switching component of the proposed controller, therefore, extends the conventional STSMC law as:

$$u_{sw} = -k_1 \mid s \mid sgn(s) - k_2 \int sgn(s)\, dt - \psi \tag{33}$$

To reduce chattering and improve convergence speed, the adaptive conditioned function $\psi$is defined through:

$$\dot{\psi} = k_3\, sgn(\psi - u_{sat}) \tag{34}$$

The saturation function u_{sat} is bounded within the interval $\pm Q$, where $Q > 0$ is determined from the design parameter k_3. It is defined as:

$$u_{sat} = \begin{cases} u, & \mid u \mid \leq Q \\ Q\, sgn(u), & \mid u \mid > Q \end{cases} \tag{35}$$

The introduction of the conditioned function ψ together with the bounded saturation function effectively mitigates chattering while maintaining fast convergence of the control signal.

To verify stability, the Lyapunov candidate defined in Eq. (25) is used. Substituting Eqs. (30) and (31) into Eq. (26) yields

$$\begin{gathered} \dot{V} = s(c_1 \dot{e}_1 + c_2 \dot{e}_2 + c_3 \dot{e}_3 \\ c_4 q_1 e_4^{q_1 - 1} e_1 + c_5 q_2 e_5^{q_2 - 1} e_2 + c_6 q_3 e_6^{q_3 - 1} e_3 \\ +c_7 e_4 + c_8 e_5 + c_9 e_6) \end{gathered} \tag{36}$$

Applying the switching law defined in Eq. (33) results in:

$$\dot{V} = s\left(-k_1 \mid s \mid sgn(s) - k_2 \int sgn(s)\, dt - \psi\right) \leq 0 \tag{37}$$

Since $\dot{V}$ is non-positive, the sliding variable converges toward zero, and the stability of the closed-loop system is guaranteed.

Finally, combining the equivalent control component in Eq. (32) with the switching term in Eq. (34) yields the overall CB-STSMC control law

$$u = u_{eq} - k_1 \mid s \mid sgn(s) - k_2 \int sgn(s)\, dt - \psi \tag{38}$$

4 Simulation and Results

The effectiveness of the proposed controllers is evaluated through numerical simulations conducted in the MATLAB/Simulink environment. The closed-loop Simulink implementation is illustrated in Figure 2, while the principal parameters of the MagLev system are summarized in Table 1. In all simulations, the control objective is to drive the system states toward the equilibrium point

$$x_* = \left[x_{1^*} \quad 0 \quad \sqrt{2kmg} \right]^T$$

where x_{1^*}represents the desired position of the levitated ball (air gap), [11].

Table 1. Model Parameters

Symbol	Description	Value	Unit
$\boldsymbol{m}$	Iron ball mass	0.068	kg
$\boldsymbol{L}$	Coil inductance	412.5	mH
$\boldsymbol{R}$	Coil resistance	10	Ω
$\boldsymbol{g}$	Gravitational acceleration	9.81	m/s²
$\boldsymbol{k}$	Coil constant	0.01838	H

Source: created by the authors

For optimal controller performance, the controller parameters must be appropriately tuned. In this study, the parameters of the proposed controllers are optimized using a GA, [16]. The GA operates by generating an initial population of candidate parameter sets and iteratively evolving them through selection, crossover, and mutation operations. At each generation, the candidate solutions are evaluated according to a predefined fitness function, and the best-performing solutions are retained for subsequent generations. The optimization process continues until the convergence criteria are satisfied.

The fitness function adopted in this work is based on the ITAE, which penalizes long-lasting tracking errors and therefore encourages faster convergence and improved transient behavior. The fitness value used during the GA optimization is defined as:

$$Fitness = \sqrt{\frac{1}{n}\sum_{i=1}^{n}\left(\int_{t_0}^{t_f} t \mid e_i(t) \mid dt\right)^2} \qquad (39)$$

where $e_i(t)$ denotes the tracking error associated with the i^{th}system state, t_0 and t_f represent the initial and final simulation times, and n is the number of controlled outputs. In the present case, $n = 3$, corresponding to the air gap, momentum, and magnetic flux states. The optimized controller parameters obtained using the GA are summarized in Table 2 (Appendix).

The simulations were conducted to evaluate the ability of the proposed controllers to track the desired air-gap reference, which is set to 2 cm and represented by the state x_1. The initial condition of the system is chosen as $x_1(0) = 1$ cm.

Figure 3(a)–3(c) illustrate the comparative dynamic responses of the system under the GA-based STSMC and GA-based CB-STSMC controllers.

Figure 3(a) shows the air-gap response. Both controllers successfully regulate the ball position to the desired reference value; however, the CB-STSMC achieves faster convergence with significantly reduced overshoot. The STSMC controller exhibits a noticeable transient overshoot and slower settling behavior before reaching the equilibrium point.

The momentum response of the iron ball is presented in Figure 3(b). The CB-STSMC controller drives the momentum to zero more rapidly and with smaller oscillations than the conventional STSMC, indicating improved damping characteristics and enhanced transient stability

Figure 3(c) depicts the magnetic flux response. The CB-STSMC controller provides a smoother flux trajectory and faster stabilization around the reference value. In contrast, the STSMC exhibits larger transient deviations before converging. This behavior confirms that the proposed controller improves the regulation of the electromagnetic dynamics of the MagLev system.

A quantitative comparison of the two control schemes is summarized in Table 3 (Appendix), which reports standard performance metrics for the air-gap response.

The results indicate that the GA-based CB-STSMC controller significantly improves the dynamic performance of the MagLev system. In particular, it achieves a faster rise time (0.1002 s compared to 0.2137 s), a shorter transient response, and a substantially reduced overshoot (0.0057 % compared to 2.3242 %). The error indices also confirm the superior performance of the proposed controller, with considerably lower ITAE and IAE values.

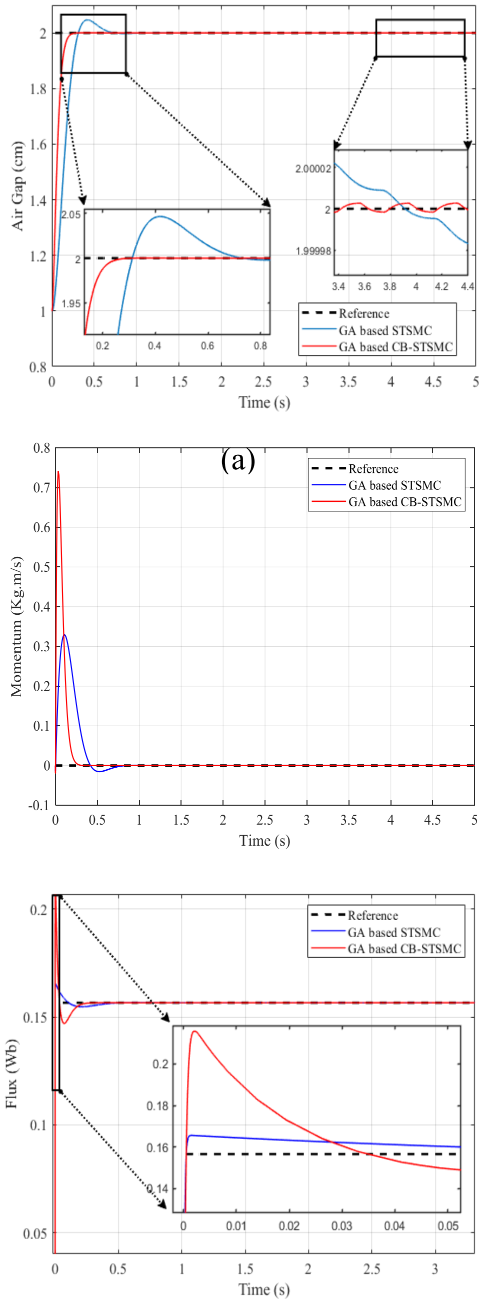

Fig. 3: Comparative Analysis of system response: (a) Air-gap, (b) the momentum of the iron ball, (c) Flux

Source: created by the authors

To evaluate the tracking quality, two integral performance indices were considered. The Integral of Absolute Error (IAE), IAE $= \int_{t_0}^{t_f} |\, e_i(t) \,|\; dt$, quantifies the overall accumulated tracking error. The Integral of Time-weighted Absolute Error (ITAE), ITAE $= \int_{t_0}^{t_f} t \,|\, e_i(t) \,|\; dt$, assigns a greater penalty to errors that persist at later times. Therefore, lower values of these indices indicate better transient behavior and faster error attenuation.

5 Conclusion

This study presented the CB-STSMC as an advanced control strategy for nonlinear MagLev systems. The proposed CB-STSMC integrates several key mechanisms, including conditioned barrier functions to maintain system operation within safe regions, adaptive components for dynamic parameter adjustment, and double-integral terminal terms to improve tracking accuracy. In addition, the incorporation of super-twisting sliding mode control principles enhances robustness against disturbances and modeling uncertainties.

The controller parameters were optimized using a GA with the ITAE selected as the optimization objective. The GA-based tuning procedure enabled effective adjustment of the controller gains, resulting in reduced steady-state error and improved transient response. Lyapunov-based analysis was used to verify the stability of the closed-loop system and to demonstrate the asymptotic convergence of the tracking errors.

Simulation results obtained in the MATLAB/Simulink environment confirmed the effectiveness of the proposed controller. Comparative analysis with the GA-based STSMC demonstrated that the CB-STSMC provides improved dynamic performance, including faster response, reduced overshoot, and better steady-state regulation of the air gap, momentum, and magnetic flux states.

Future work will focus on extending the proposed approach toward real-time implementation on a physical MagLev platform, as well as investigating robustness under external disturbances, parameter uncertainties, and hardware constraints. Additional research may also explore improved GA tuning strategies and alternative optimization techniques to further enhance controller performance.

References:

[1] L. Yan, "Development and application of the maglev transportation system," IEEE Transactions on Applied Superconductivity, vol. 18, no. 2, pp. 92–99, 2008, https://doi.org/10.1109/TASC.2008.922239.

[2] S. Palagummi, F.-G. Yuan, "Magnetic levitation and its application for low-frequency vibration energy harvesting," in Structural Health Monitoring (SHM) in Aerospace Structures, Elsevier, 2016, pp. 213–251, https://doi.org/10.1016/B978-0-08-100148-6.00008-1.

[3] H. Yaghoubi, "The Most Important Maglev Applications," *Journal of Engineering*, vol. 2013, no. 1, Art. no. 537986, 2013, doi: https://doi.org/10.1155/2013/537986

[4] C. Shuangxi, "Comprehensive degree of nonlinearity in the dynamic response of high-speed maglev train," Measurement and Control, vol. 58, no. 3, pp. 295–308, 2024, https://doi.org/10.1177/00202940241253940.

[5] B. Ataşlar-Ayyıldız, O. Karahan, "Design of a MAGLEV system with PID-based fuzzy control using CS algorithm," Cybernetics and Information Technologies, vol. 20, no. 5, pp. 5–19, 2020, https://doi.org/10.2478/cait-2020-0037.

[6] R.-J. Wai, J.-X. Yao, J.-D. Lee, "Backstepping fuzzy-neural-network control design for hybrid maglev transportation system," IEEE Transactions on Neural Networks and Learning Systems, vol. 26, no. 2, pp. 302–317, 2015, https://doi.org/10.1109/TNNLS.2014.2314718.

[7] A. S. Malik, I. Ahmad, A. U. Rahman, Y. Islam, "Integral backstepping and synergetic control of magnetic levitation system," IEEE Access, vol. 7, pp. 173230–173239, 2019, https://doi.org/10.1109/ACCESS.2019.2952551.

[8] A. Mughees, I. Ahmad, N. Mughees, A. Mughees, "Conditioned adaptive barrier-based double integral super twisting SMC for trajectory tracking of a quadcopter and hardware in loop using IGWO algorithm," Expert Systems with Applications, vol. 235, Article no. 121141, 2024, https://doi.org/10.1016/j.eswa.2023.121141.

[9] H. M. M. Adil, S. Ahmed, I. Ahmad, "Control of MagLev system using supertwisting and integral backstepping sliding mode algorithm," IEEE Access, vol. 8, pp. 51352–51362, 2020, https://doi.org/10.1109/ACCESS.2020.2980687.

[10] H. M. S. Yaseen, S. A. Siffat, I. Ahmad, A. S. Malik, "Nonlinear adaptive control of magnetic levitation system using terminal sliding mode and integral backstepping sliding mode controllers," ISA Transactions, vol. 126, pp. 121–133, 2022, https://doi.org/10.1016/j.isatra.2021.07.026.

[11] R. Ortega, A. J. van der Schaft, I. Mareels, B. Maschke, "Putting energy back in control," IEEE Control Systems Magazine, vol. 21, no. 2, pp. 18–33, 2001, https://doi.org/10.1109/37.915398.

[12] D. Xu, Q. Liu, W. Yan, W. Yang, "Adaptive terminal sliding mode control for hybrid energy storage systems of fuel cell, battery and supercapacitor," IEEE Access, vol. 7, pp. 29295–29303, 2019, https://doi.org/10.1109/ACCESS.2019.2897015.

[13] H. Bayramoglu, H. Komurcugil, "Time-varying sliding-coefficient-based decoupled terminal sliding-mode control for a class of fourth-order systems," ISA Transactions, vol. 53, no. 4, pp. 1044–1053, 2014, https://doi.org/10.1016/j.isatra.2014.05.013.

[14] S. S.-D. Xu, "Super-twisting-algorithm-based terminal sliding mode control for a bioreactor system," Abstract and Applied Analysis, vol. 2014, Article ID 495680, pp. 1–9, 2014, https://doi.org/10.1155/2014/495680.

[15] A. Mohammadpour Shotorbani, E. Babaei, "Robust nonlinear controller based on control Lyapunov function and terminal sliding mode for buck converter," International Journal of Numerical Modelling: Electronic Networks, Devices and Fields, vol. 29, no. 6, pp. 1055–1069, 2016, https://doi.org/10.1002/jnm.2164.

[16] B. Bekkar, K. Ferkous, "Design of online fuzzy tuning LQR controller applied to rotary single inverted pendulum: Experimental validation," Arabian Journal for Science and Engineering, vol. 48, no. 5, pp. 6957–6972, 2023, https://doi.org/10.1007/s13369-022-06921-3.

Contribution of Individual Authors to the Creation of a Scientific Article (Ghostwriting Policy)

Belgacem BEKKAR contributed to the conceptualization of the study, development of the control methodology, controller design, simulation implementation in MATLAB/Simulink, analysis and interpretation of the results, and preparation of the original manuscript draft.

Khaled FERKOUS contributed to the supervision of the research work, validation of the theoretical analysis, critical review and editing of the manuscript, and overall guidance of the study.

Both authors reviewed and approved the final version of the manuscript.

Sources of Funding for Research Presented in a Scientific Article or Scientific Article Itself

No funding was received for conducting this study.

Conflict of Interest

The authors have no conflicts of interest to declare that are relevant to the content of this article.

APPENDIX

Table 2. Optimized Controller Gain Parameters

Controller	Gains	Values
GA-based STSMC	k_1, k_2	164, 6.94
	c_1, c_2, c_3	30.92, 60.48, 34.88
GA-based CB-STSMC	k_1, k_2, k_3	194.72, 2.97, 2.95
	c_1, c_2, c_3, c_4	73.44, 64.61, 16.85, 60.74
	c_5, c_6, c_7, c_8, c_9	89.39, 98.05, 30.37, 30.95, 33.55
	q_1, q_2, q_3	1.28, 1.43, 1.53

Source: created by the authors

Table 3. Comparative Performance Metrics of Proposed Controllers for Air-Gap Response

Metric	GA-based STSMC	GA-based CB-STSMC
Rise Time (s)	0.2137	0.1002
Transient Time (s)	0.5697	0.1845
Settling Time (s)	0.4768	0.1613
Overshoot (%)	2.3242	0.0057
Peak	2.0465	2.0001
Peak Time (s)	0.4188	0.3600
ITAE	2.0930×10^{-4}	3.3400×10^{-5}
IAE	0.0016	6.7030×10^{-4}

Source: created by the authors